Solid Earth, 14, 785–803, 2023
https://doi.org/10.5194/se-14-785-2023

Solid Earth Open Access EGU

Ground motion emissions due to wind turbines: observations, acoustic coupling, and attenuation relationships

Laura Gaßner and Joachim Ritter

Geophysical Institute, Karlsruhe Institute of Technology, Hertzstraße 16, 76187 Karlsruhe, Germany

Correspondence: Laura Gaßner (laura.gassner@kit.edu)

Received: 28 March 2022 – Discussion started: 12 May 2022
Revised: 31 May 2023 – Accepted: 4 June 2023 – Published: 18 July 2023

Abstract. Emissions from wind turbines (WT) cover a wide range of infrasound and ground motions. When they are perceived as *immissions* by local residents, they can become a source of disturbance or annoyance. To mitigate such disturbances, it is necessary to better understand and, if possible, suppress WT-induced emissions. Within the project Inter-Wind we record and analyze ground motion signals in the vicinity of two wind farms on the Swabian Alb in southern Germany, simultaneously with acoustic and meteorological measurements, as well as psychological surveys done by cooperating research groups. The investigated wind farms consist of 3 and 16 WTs, respectively, and are located on the Alb peneplain at 700–800 m height, approximately 300 m higher than the two municipalities considered in our study. Our main aim is to better understand reasons why residents may be affected from WT immissions.

Known ground motions include vibrations due to eigenmodes of the WT tower and blades, and the interaction between the passing blade and the tower, causing signals at constant frequencies below 12 Hz. In addition, we observe signals in ground motion recordings at frequencies up to 90 Hz which are proportional to the blade-passing frequency. We can correlate these signals with acoustic recordings and estimate sound pressure to ground motion coupling transfer coefficients of 3–16.5 $\mu m\,s^{-1}\,Pa^{-1}$. Sources for these emissions are the WT generator and possibly the gearing box. The identification of such noise sources can help to find measures to reduce disturbances in order to increase the public acceptance of WTs. Residents perceive more disturbance at the location where the wind farm is closer to the municipality (approximately 1 km). However, there is also a major railway line which produces higher vibration and infrasound signal amplitudes compared to the WTs.

Along the measurement lines the decay rate of the WT-induced ground motions is determined for a damping relation proportional to $1/r^b$. We find frequency-dependent b values for different scenarios at our geological setting of Jurassic limestone on marl, sandstone, and Quaternary deposits. These damping relationships can be used to estimate emissions in the far field and to plan mitigation strategies.

1 Introduction

To achieve a transition to renewable energies an increased utilization of wind energy is necessary. In Germany the number of newly installed wind turbines (WTs) increased to more than 2000 (> 1 MW) per year in 2017, but it dropped to roughly 20 % of that number in the following years (Bundesnetzagentur, 2022). The drop in expansion can be related to more restrictions (e.g., in Bavaria the distance to dwellings must be 10 times the total height of the WT) and/or protests of conservationists and residents. Opponents protest against environmental, visual, and acoustic aspects of WT installation and operation due to a feared loss of their quality of life. Due to lawsuits many WT projects are delayed significantly (FA Wind, 2019). WT emissions may also influence technical operations such as high-resolution electron microscopes, air traffic control, or seismological observatories. A reduction of WT emissions requires an understanding of the source, propagation, and arrival of ground motions. In this study we derive general properties of WT emissions based on dedicated highly sensitive field experiments.

Within the project Inter-Wind we aim to classify which properties of WT operation could be responsible for the annoyance of residents in the vicinity of two wind farms on the

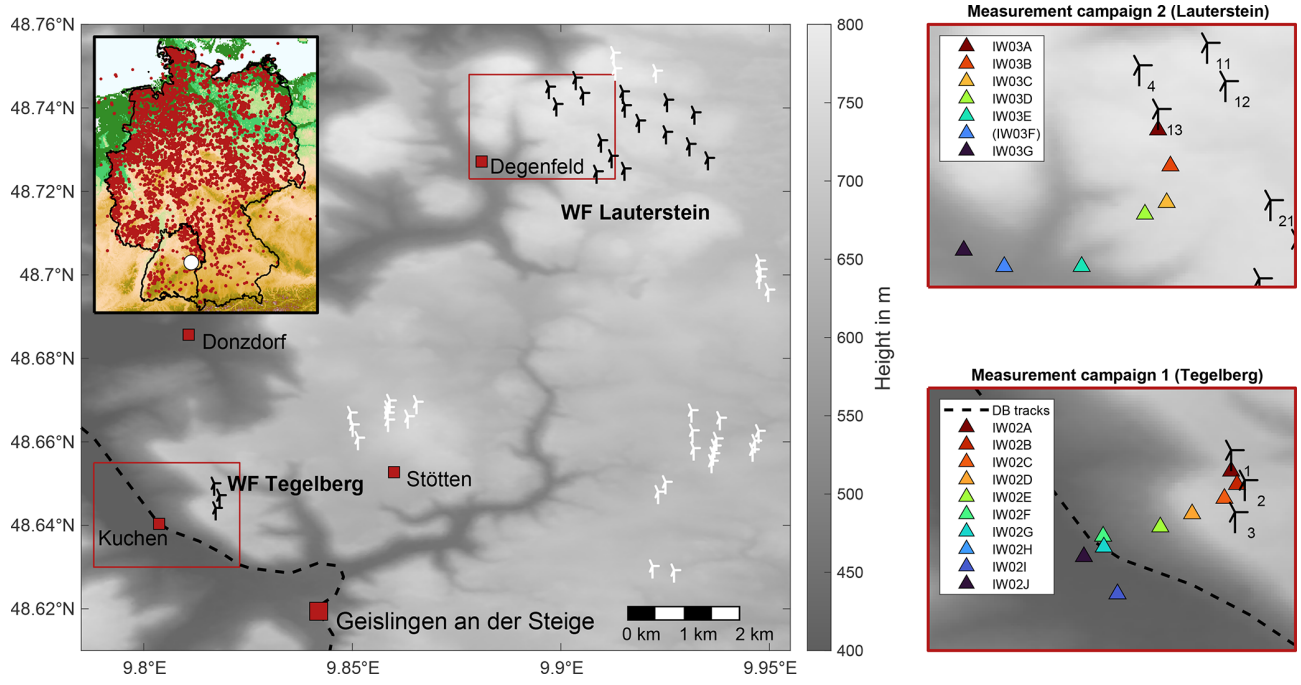

Figure 1. Inter-Wind study area with relevant places and locations of WTs (black – part of this study, white – no operating data available). Inset: map of Germany with the outline of the state of Baden-Württemberg. The white marker denotes the location of the project area; dark-red dots mark German WT positions (Bundesnetzagentur, 2022). Detailed maps show the recording station positions (colored triangles) for measurement campaigns at wind farms Tegelberg (bottom) and Lauterstein (top). The dashed line (DB tracks) is the main railway line Stuttgart–Ulm.

Swabian Alb, a mountain range in SW Germany (Fig. 1). Beside psychological questionnaires we measure meteorological, acoustic, and ground motion data, which build the foundation for an interdisciplinary analysis (Gaßner et al., 2022). In this paper we concentrate on the seismological perspective, focusing on induced ground motions of WTs. These are caused by the coupling of the WT foundations with the ground (Nagel et al., 2021) and are expected not to be perceptible by humans (e.g., Ratzel et al., 2016). Regulations for the impact of vibrations on humans in buildings are defined in DIN 4150-2 (1999), stating a relevant frequency range of 5.6 to 80 Hz. As a lower limit for perceptible signals, typically a value of 0.1 mm s^{-1} (= 100 µm s^{-1}) is taken, derived from specifications in DIN 4150-2, Table 1. Although these amplitudes are unlikely to be reached, surveys of residents living near wind farms have shown that vibrations are named as an annoying property of WT operation (e.g., Michaud et al., 2016), and measured data are needed to provide local vibration amplitudes.

Signals emitted by WTs are related to the eigenmodes of the WT tower and blades (Nagel et al., 2021; Zieger et al., 2020), as well as the blade-passing frequency (BPF) and its multiples (e.g., Styles et al., 2005; Nagel et al., 2021; Neuffer et al., 2021). While the latter are proportional in frequency to the rotation rate of the WT, natural vibrations due to eigenmodes are of constant frequency and increase in amplitude with higher rotation rates. Typically the emitted ground motions were studied for frequencies below 20 Hz. Lower frequencies are attenuated less than higher frequencies and can be detected up to distances of more than 10 km (e.g., Schofield, 2001; Saccorotti et al., 2011). Seismic signals caused by WT operation are studied eagerly in the seismological community, as they disturb sensitive measurements, e.g., monitoring networks (Styles et al., 2005; Stammler and Ceranna, 2016; Estrella et al., 2017; Neuffer and Kremers, 2017; Zieger and Ritter, 2018).

Our ground motion measurements were conducted within two campaigns aimed at characterizing WT signals in the vicinity of two wind farms. They were set up in combination with acoustic measurements to provide a data basis to evaluate annoyance reports of local residents (Gaßner et al., 2022). The wind farms under investigation are located on the Swabian Alb, near Geislingen an der Steige (Fig. 1), and consist of 3 (Tegelberg) and 16 (Lauterstein) WTs of the same type, respectively. The WT type is a General Electric (GE) 2.75-120 with 139 m hub height, 120 m rotor diameter, and 2.78 MW rated power. Because there is much less reported annoyance at wind farm Lauterstein compared to wind farm Tegelberg, we focus mostly on the analysis of signals measured at wind farm Tegelberg in this study. Additionally, acoustic measurements are directly co-located there.

Table 1. Sensors (Streckeisen STS-2, Nanometrics Trillium Compact Posthole (TC-PH), Lennartz LE-3D) with their respective eigen-period and data loggers (Earth Data PR6-24 Portable Field Recorder (EDL), DiGOS DATA-CUBE^3, Nanometrics Centaur Digital Recorder) used for the measurement campaigns at Tegelberg (IW02) and Lauterstein (IW03).

	Sensor			Data logger		
	STS-2 120 s	TC-PH 20 s	LE-3D 1 s	EDL	CUBE	Centaur
IW02A	x	–	–	x	–	–
IW02B, C	–	–	x	–	x	–
IW02D, E	–	x	–	–	x	–
IW02F, G, H, I, J	–	x	–	–	–	x
IW03A, F	–	x	–	–	–	x
IW03B, C, D	–	x	–	–	x	–
IW03E, G	–	–	x	–	x	–

2 Measurements

We installed 7 to 10 seismic recording stations in profile-like setups (Fig. 1). For comparability, we chose profiles of southwest–northeast orientation to achieve an observational connection between the place of emission (near the WTs) and immission (at local residents) at both wind farms. Both profiles are located across significant changes in elevation, the so-called Alb Cuesta: the WTs are placed on the Alb peneplain at approx. 700 to 800 m elevation on the Kimmeridgian limestone (Upper Jurassic), whereas the villages of Kuchen and Degenfeld are located in the valley at ca. 400 m on Quaternary deposits overlying marl and sandstones (Middle Jurassic) and at ca. 500 m on Quaternary deposits overlying marl (Lower Jurassic), respectively. At wind farm Tegelberg with three WTs, a total recording time of 3.5 months was achieved with five stations at the wind farm and the surrounding forest, plus four 2-week-long measurements at the residents in the municipality of Kuchen in the first half of the measurement campaign. At wind farm Lauterstein 4 to 6 weeks of measurements were conducted, with a total of seven stations (five field stations and two in Degenfeld).

Close contact with the WT operators was established to support measurements and signal analysis and to provide WT operating data, like rotation rate, wind speed, and wind direction. These WT operating data were averaged over 10 min time windows. For each campaign one recording station was installed inside the tower of one WT, at the outermost edge of the tower interior. The other stations were placed in a profile-like setup towards the nearest settlement, i.e., where complaints were registered. Within these communities residents had been surveyed via psychological questionnaires earlier to find participants offering their houses for further measurements (Gaßner et al., 2022).

Details on the instrumentation of each recording station are summarized in Table 1. CUBE^3 data loggers were utilized for all field stations where there was no power available. These recording stations were mostly buried in the ground in approximately 30 cm depth for insulation (except IW03G which was installed inside a cellar). For the campaign in Tegelberg recorders were set to a sampling rate of 100 Hz; in Lauterstein 200 Hz was used in order to also capture higher-frequency emissions which were observed in the Tegelberg campaign.

After a general comparison of signals measured at both wind farms, we analyze signals from wind farm Tegelberg in more detail. One reason is that ground motion data were measured directly next to the acoustic recording equipment there (at the wind farm and also at the resident sites). At wind farm Lauterstein there were no directly co-located measurements. Another reason is the high number of noise reports related to wind farm Tegelberg, making this the more interesting study site.

2.1 Wind farm Tegelberg

The first measurement campaign at wind farm Tegelberg took place from 20 October 2020 to 5 February 2021, amounting to 108 d. In total we deployed 10 recording stations, of which 1 station (IW02A) was installed in the tower of WT 1, 1 station (IW02B) near an acoustic measurement site in approximately 150 m distance to WT 1, and 3 more stations in the forest surrounding the wind farm (IW02C-E, at 150 to 550 m distance to the nearest WT). Additionally, we conducted 2-week-long measurements outside four resident houses (IW02F-J) and in the basement of resident 3 (IW02H) in Kuchen. The distribution of the recording stations towards the southwest, as seen from the wind farm, is shown in Fig. 1. Wind farm Tegelberg belongs to the town of Donzdorf and is located approximately 4.5 km to the south of it. The average distance of the affected residents in Kuchen to the wind farm is 1 km. Between the inhabited area in the valley and the wind farm Tegelberg, there is a difference in topography of approximately 300 m.

Figure 2a gives an overview of the relation between rotation rates and wind speed at WT 1 of wind farm Tegelberg. Furthermore, the wind direction distribution is shown, exhibiting a dominance of westerly wind conditions. Rota-

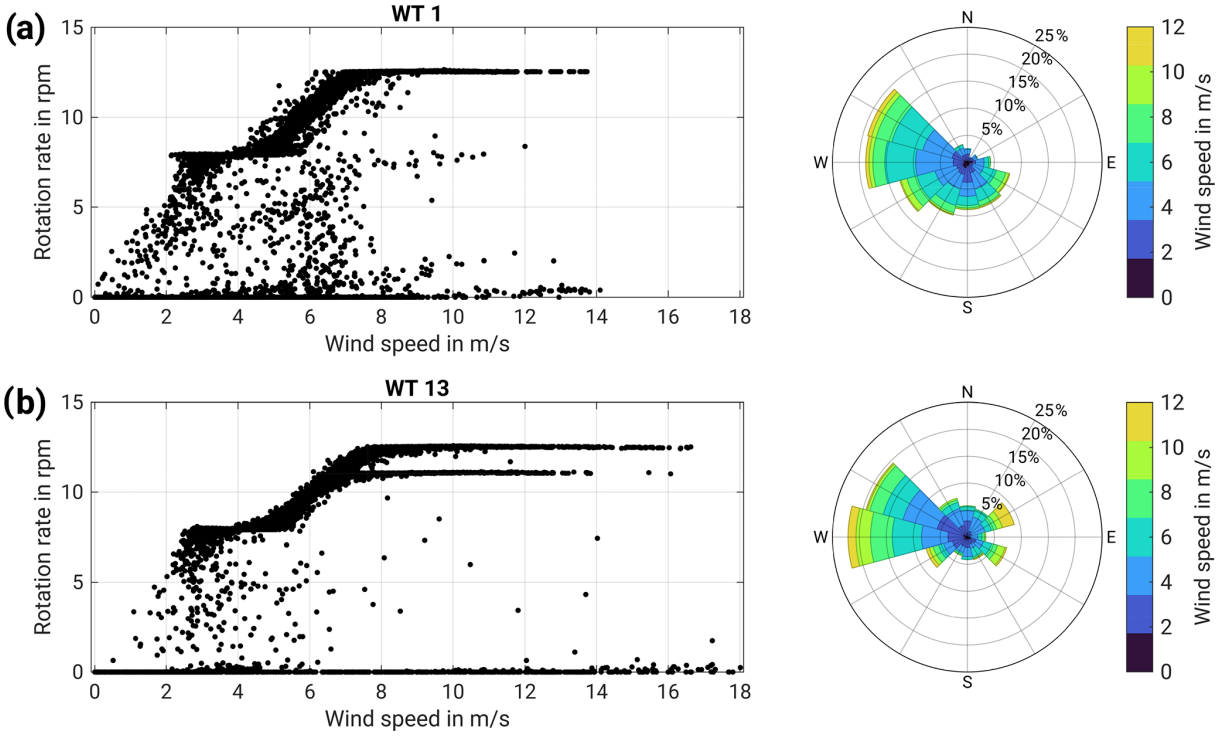

Figure 2. Operating data for **(a)** WT 1 of wind farm Tegelberg and **(b)** WT 13 of wind farm Lauterstein. Left: rotation rate vs. wind speed. Right: wind rose for the wind speed and direction distribution during the measurement period. The outer circle represents 25 % occurrence, indicating that W and WNW were the main wind directions with approx. 19 % (Tegelberg) and 22 % and 19 % (Lauterstein) likelihood each.

tion rates for the considered turbine type typically reach up to 12.5–12.6 rpm (rotations per minute) during full operation at wind speeds above 6 m s^{-1}, which corresponds to 0.625–0.630 Hz primary BPF. Additionally, a plateau at 7.9–8 rpm can be observed, corresponding to a BPF of 0.395–0.400 Hz, related to wind speeds between 2 and 6 m s^{-1}. For the other two WTs at Tegelberg similar observations can be made. During nighttime (21:00 to 05:00 UTC, 22:00 to 06:00 local time) WT 3 runs in a noise-reduced mode to mitigate acoustic emissions, resulting in a maximum of 12 rpm at full load (0.6 Hz BPF).

2.2 Wind farm Lauterstein

At wind farm Lauterstein measurements were conducted for 46 d, from 22 February 2021 to 8 April 2021. We deployed seven recording stations, though at one station only very limited data could be recovered due to problems with the sensor (IW03F). Again, one recording station was installed inside the tower, close to the wall of WT 13 (IW03A, Fig. 1), and three stations in the surrounding forest (IW03B-D), at distances of 400 to 900 m to WT 13. Additionally, one station was set up near the village Degenfeld (IW03E, 1.5 km to WT 13) and one station inside a community building (IW03G, 1.9 km to WT 13). As no significant complaints were reported with regard to emissions from wind farm Lauterstein, no affected residents took part in the campaign.

A noise-reduced mode is implemented at WT 13, due to a dwelling at 550 m distance. This leads to rotation rates limited to 11 rpm (0.55 Hz BPF) during nighttime (Fig. 2b). Two more WTs (WT 12 and WT 21, Fig. 1) close to WT 13 also have noise-reduced operation, with maximum rotation rates at 11.5 rpm (0.575 Hz BPF) at night. Wind direction distribution at Lauterstein (Fig. 2b) is similar to wind farm Tegelberg, with west to west-northwest the dominant direction.

3 Ground motion signals

From the raw data recovered with our recorders, the true ground motion is calculated by removing the instrument response using the *ObsPy* (Krischer et al., 2015) package and the respective instrument information. A two-pole bandpass filter is then applied with corner frequencies of 0.1 and 45 or 95 Hz, for data from Tegelberg and Lauterstein, respectively. We calculate power spectral densities (PSDs) based on the method of Welch (1967), taking 60 s time windows with an overlap of 20 s.

Typical signals measured in the vicinity of wind farms are the eigenmodes of the WT tower and blades (Nagel et al., 2021), which are of constant frequency and exhibit amplitudes proportional to the rotation rate of the WT. The eigen-

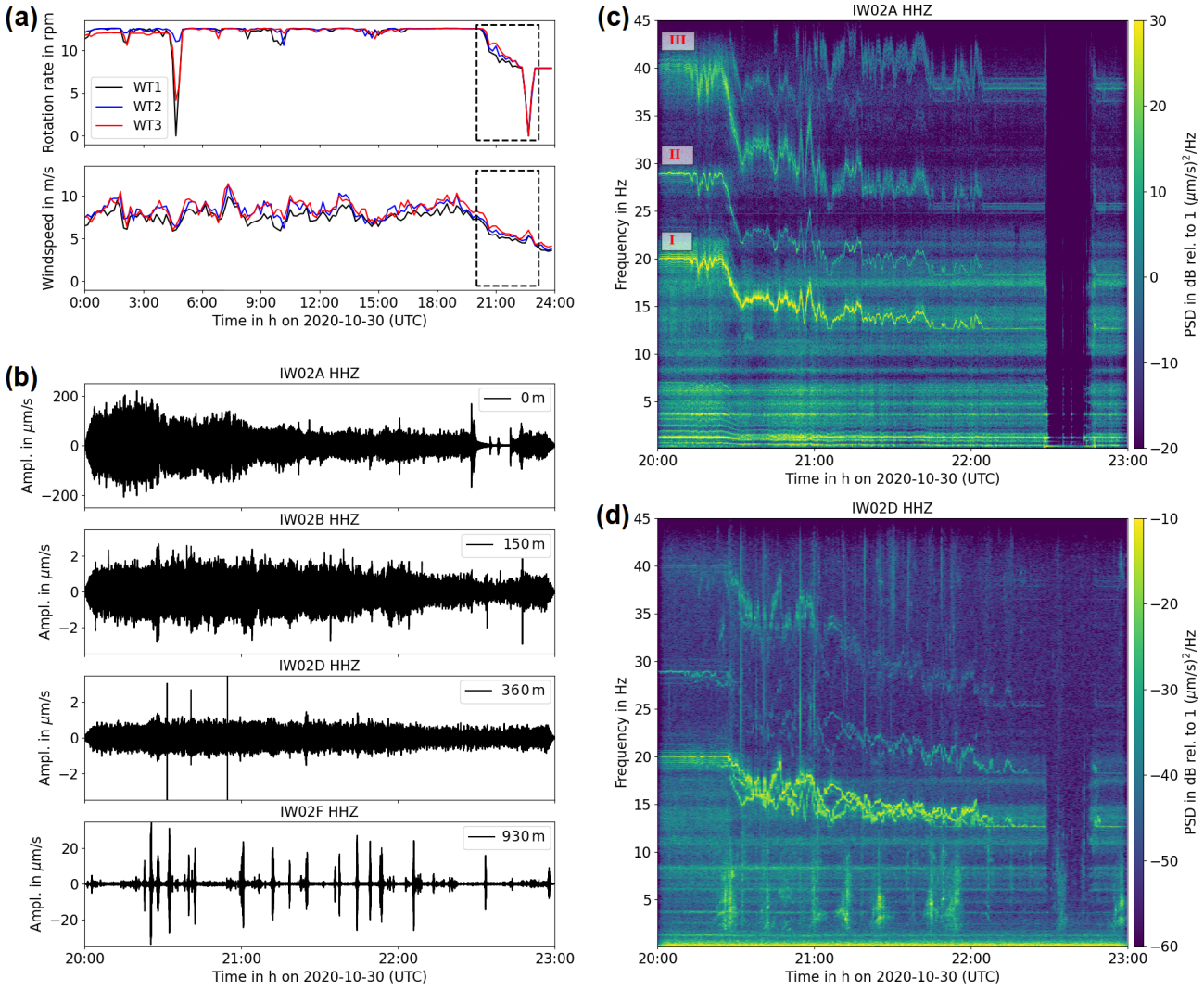

Figure 3. **(a)** Operating data (rotation rate and wind speed) of the three WTs at wind farm Tegelberg for 30 October 2020. The dashed black box indicates the time window chosen for **(b–d)**; **(b)** 3 h time series of the vertical ground motion for stations IW02A, IW02B, IW02D, and IW02F, with the respective distance to the nearest WT. Note the different amplitude scales. **(c)** PSD spectrogram for the vertical ground motion of IW02A inside the tower of WT 1 for the same 3 h time window as **(b)**. **(d)** Same as **(c)** for recording station IW02D, located at approximately 360 m distance to WT 3.

modes occur mainly at frequencies below 12 Hz and, as they are less damped than higher frequencies, are therefore detectable over long distances (Saccorotti et al., 2011). Such signals lead to a potential reduction of detection capabilities of monitoring networks, e.g., for microseismicity (Neuffer and Kremers, 2017). As we study two wind farms consisting of the same turbine type, we expect to find the same frequencies in both measurements.

In Fig. 3 we present an overview of ground motion signals recorded during a 3 h time window at wind farm Tegelberg (20:00–23:00 UTC, 21:00–24:00 LT). It includes a drop in rotation rate of all three WTs (20:30 UTC), with a time interval when all WTs shut down (at 22:30 UTC) and then restart after approx. 15 min (Fig. 3a). The reduction of rotation rate can be explained by a drop in wind speed from approx. 8 to 5 $\mathrm{m\,s^{-1}}$. It is not obvious why the WTs turned off completely for a short time, though. Typically, the detection of protected species, e.g., bats or red kites, in the vicinity of the WTs can be a reason for sudden automated shutdowns. The reduction in rotation rate is visible in the ground motion data (Fig. 3b), and as expected the change in amplitude is less pronounced with increasing distance of the recording stations to the WTs. At 360 m distance ground motion signal amplitudes are approximately 1 $\mathrm{\mu m\,s^{-1}}$ during WT operation.

In the spectrograms the signals and their relation to frequency can be observed well, for the station inside WT 1 (IW02A, Fig. 3c) and a site at approx. 360 m distance to the next WT (IW02D, Fig. 3d). At IW02D signals proportional

in frequency to the BPF are visible for each WT between 20:30 UTC and 22:00 UTC when the rotation rate fluctuates between 12.5 and 8 rpm. One of the observed signals corresponds to the generator speed with frequencies at 46 × BPF (II, Table 2); other signals are at 32 × (I), and 64 × BPF (III). They are most prominent for the two main rotation rates in the operating range, at 8 and 12.5 rpm. A more detailed study of these signals can be found in Sect. 3.1 for wind farm Tegelberg.

Additionally, in Fig. 3d signals are visible that only last for a few minutes and occur mainly at frequencies below 10 Hz. They are related to the train traffic in the valley where Kuchen is located and are especially prominent at the resident locations (IW02F in Fig. 3b). At this location the train signals reach ground motion amplitudes of more than 20 $\mu m\,s^{-1}$. A more detailed discussion of these signals can be found in section 3.2.

At wind farm Lauterstein we have a wider spread of recording sites as well as WT distribution. Here, during a drop in wind speed (Fig. 4a), which leads to a reduction of rotation rates, we observe a visible reduction in ground motion signal amplitude for the station inside WT 13 (Fig. 4b). At the recording stations outside the WT there is only a very small reduction in ground motion amplitude. The spectrograms (Fig. 4c and d) indicate that signal amplitudes related to the BPF are low outside the WT. Here, additional signals at 96 × (IV) and 128 × BPF (V) can be observed, due to the higher sampling rate of 200 Hz at wind farm Lauterstein compared to 100 Hz for measurements at wind farm Tegelberg. The respective frequencies for these signals are listed in Table 2.

Figure 5 shows a direct comparison of ground motion spectra inside the WT towers, for sites at the outermost edge of the tower interior (IW02A in WT 1 and IW03A in WT 13 at wind farms Tegelberg and Lauterstein, respectively) and at approx. 360 and 390 m distance (IW02D and IW03B). Data of 2–3 d with full operation of the whole wind farms were considered for the calculation of the spectra. Both the spectra of ground motion inside the WT tower and in the free field at less than 400 m distance agree considerably well. The highest similarity can be observed for frequencies below 5 Hz (enlarged box in Fig. 5), while at higher frequencies the spectra for IW02D and IW03B differ by 5–25 dB. This difference can be explained by the slightly smaller distance (360 m compared to 390 m) to the respective WT for IW02D and the increased background signal level due to the proximity to Kuchen and the train tracks. A difference of up to 17 dB is visible for IW02A and IW03A at frequencies higher than 22 Hz.

3.1 Signals at place of emission

Amplitudes of the WT-induced signals are generally proportional to the rotation rate, which in turn is related to the wind speed as shown in Fig. 2. Exemplary, we show spectra for recording station IW02B (150 m from WT 1 at wind farm Tegelberg) for 2 weeks of data in Fig. 6, for rotation rates of 8 and 12.5 rpm. Below 12 Hz we observe an increase of PSD values with rotation rate. Between 12 and 20 Hz PSD values do not increase for higher rotation rates but exhibit peaks at different frequencies for different rotation rates. A significant peak can be observed at 28.9 Hz for 12.5 rpm and further increased PSD values between 33 and 42 Hz. These spectral values correspond to signals with frequencies proportional to the BPF (above 12 Hz). As mentioned before, signals occur at 46 × BPF (generator speed) and at multiples of 32 × BPF (Table 2). In Fig. 6 we find that the peak at 64 × BPF is slightly smaller than a peak at 65 × BPF which is considered for the choice of frequencies in the following evaluation. Signals from the other WTs, potentially operating at different rotation rates, can be present. Furthermore, it has to be noted that rotation rates are averaged over 10 min time windows and, therefore, can span a larger rotation rate range.

To study further dependencies of signal amplitudes, we choose 25 segments lasting 2–17 h from 45 d (29 October 2020 to 12 December 2020) with rotation rates either constant at 8 rpm (549 segments of 10 min) or 12.5 rpm (366 segments of 10 min) and analyze the maximum vertical ground motion velocity (v_Z) values for three dominant frequencies per rotation rate. These frequencies are 12.5, 18, and 26 Hz for 8 rpm, as well as 20, 29, and 41 Hz for 12.5 rpm. Amplitude values are taken from data filtered in frequency bands of ± 1 Hz relative to the dominant frequencies.

We observe a distribution of amplitudes dependent on different wind direction segments (Fig. 7). For rotation rates of 8 rpm, there are four distinct angular segments (E, S,

Table 2. Frequencies corresponding to multiples of the BPF for the primary rotation rates of 7.9–8 and 12.5–12.6 rpm and labels I–V used in Figs. 3 and 4. For simplicity values are provided for 8 and 12.5 rpm only.

	8 rpm [Hz]	12.5 rpm [Hz]
1 × BPF	0.4	0.625
2 × BPF	0.8	1.250
3 × BPF	1.2	1.875
4 × BPF	1.6	2.500
5 × BPF	2.0	3.125
6 × BPF	2.4	3.750
7 × BPF	2.8	4.375
8 × BPF	3.2	5.000

Label		8 rpm [Hz]	12.5 rpm [Hz]
I	32 × BPF	12.8	20.000
II	46 × BPF	18.4	28.750
III	64 × BPF	25.6	40.000
IIIa	65 × BPF	26.0	40.625
IV	96 × BPF	38.4	60.000
V	128 × BPF	51.2	80.000

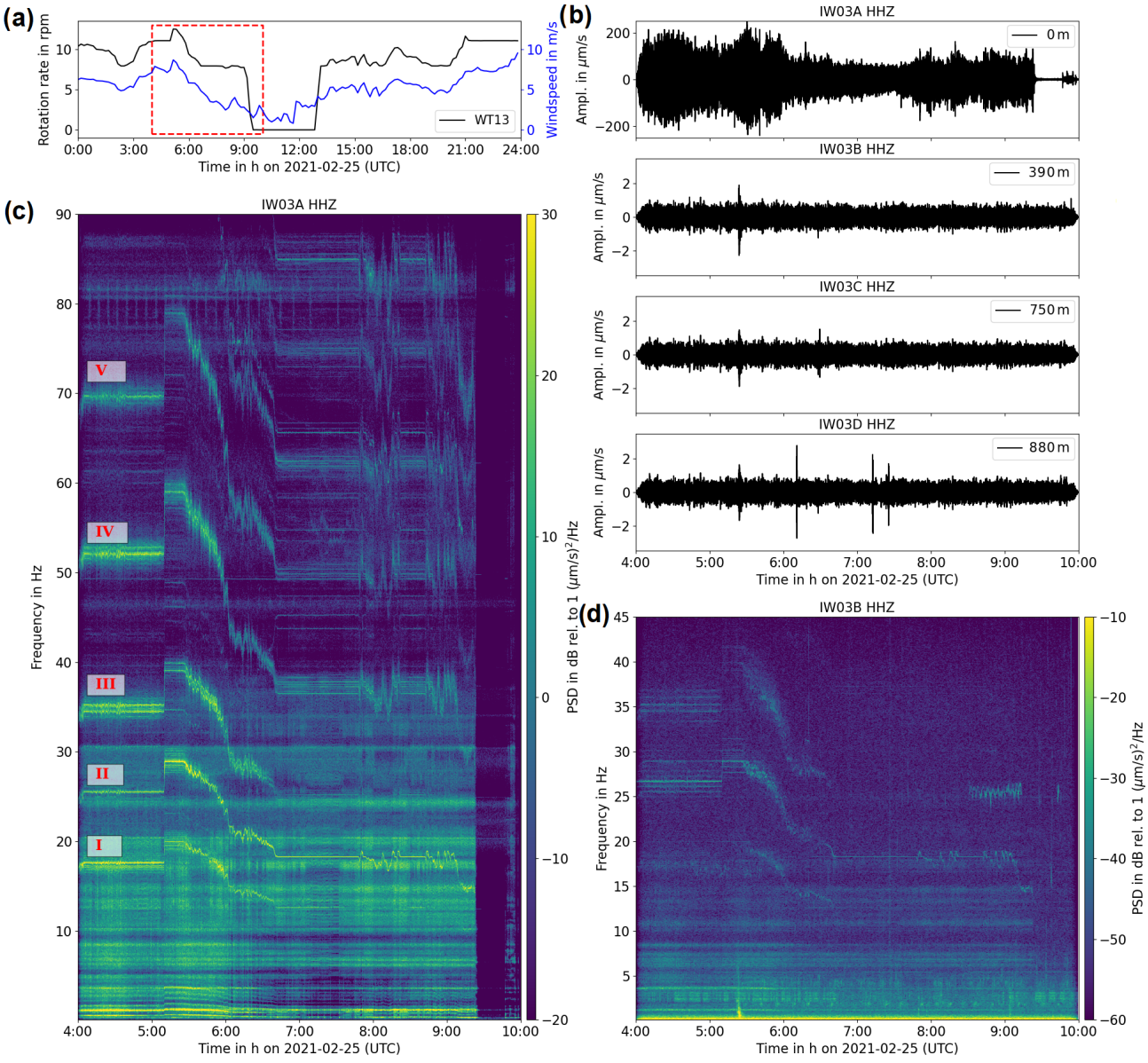

Figure 4. **(a)** Operating data (rotation rate and wind speed) of WT 13 at wind farm Lauterstein for 25 February 2021. The dashed red box indicates the time window chosen for **(b–d)**; **(b)** 6 h time series of the vertical ground motion for recording stations IW03A, IW03B, IW03C, and IW03D, with the respective distance to the nearest WT. **(c)** PSD spectrogram for the vertical ground motion of IW03A inside the tower of WT 13 for the same 6 h time window as **(b)**. **(d)** Same as **(c)** for station IW03D, located in approximately 390 m distance to WT 13.

W, and NW), while for 12.5 rpm there are only two zones (SE and W), which implies that winds strong enough to achieve full WT operation originate either in western or southeastern direction. The amplitudes of the generator frequency signals correspond to the first or second multiple of $32 \times$ BPF, 12.5 Hz ($32 \times$ BPF at 8 rpm) and 41 Hz ($64 \times$ BPF at 12.5 rpm), respectively. The WT is located at $-17°$ relative to north as seen from IW02B.

3.2 Signals at place of immission

As the main focus of our research project lies on how local residents experience WT emissions, we recorded 2 weeks of data at four different locations within the municipality of Kuchen. The measured ground motion signals, though, are dominated by the train traffic, with trains passing through the valley in intervals of several minutes, even at nighttime (Fig. 3b, IW02F). Due to the high frequency of train passages, an assignment to WT operating conditions with data available for 10 min intervals is therefore not meaningful.

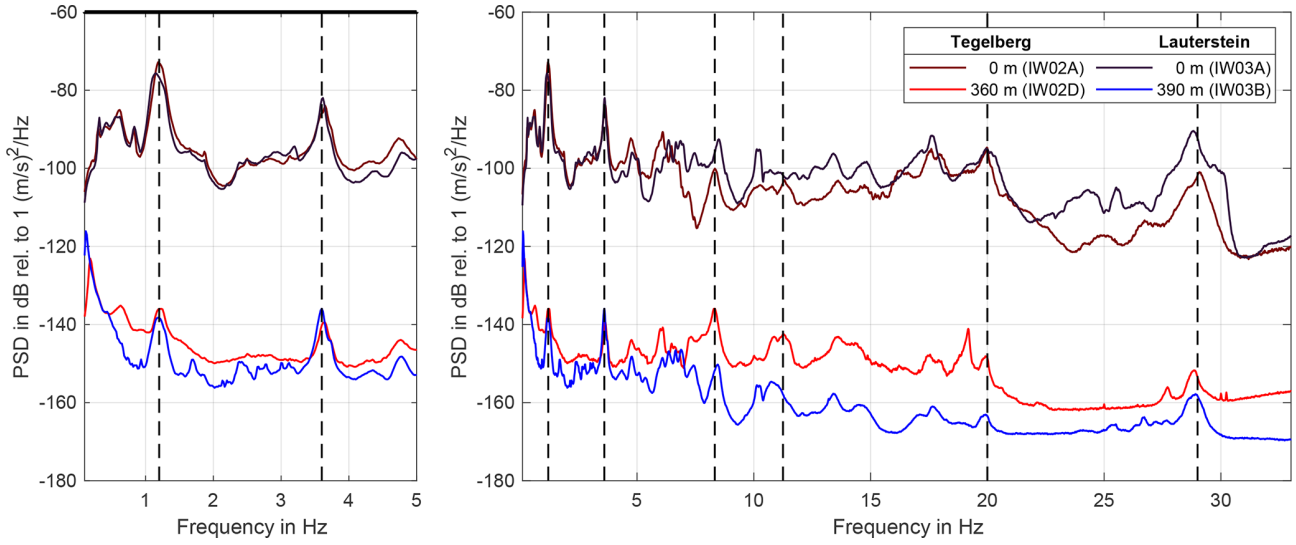

Figure 5. Comparison of mean PSD spectra for recordings inside the WT tower (upper curves) and close by in the free field (lower curves) for measurement campaigns Tegelberg (IW02, red colors, distance 360 m) and Lauterstein (IW03, blue colors, distance 390 m). For Tegelberg all three WTs were in full operation for approximately 2 d. At Lauterstein all 16 WTs were in full operation for almost 3 d. Frequencies considered for amplitude decay analysis are marked by dashed black lines.

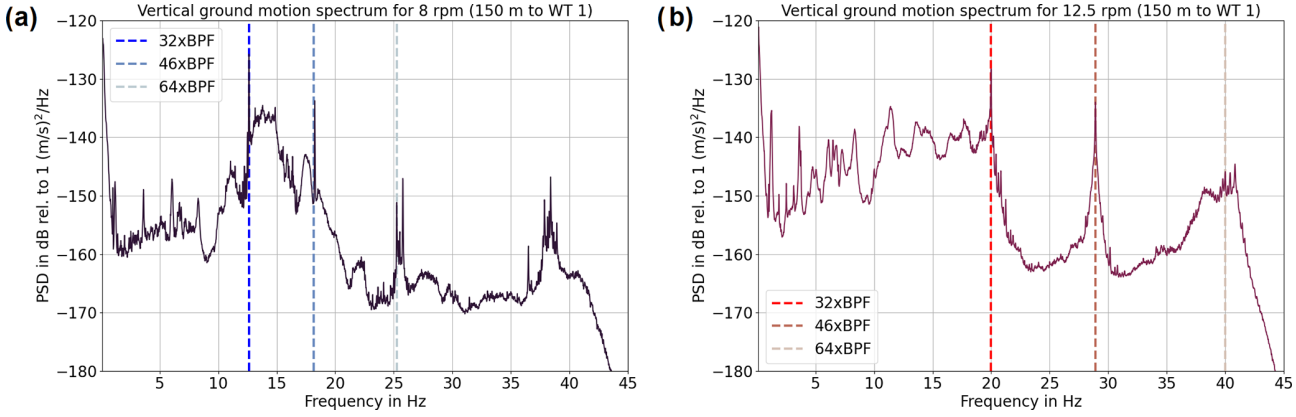

Figure 6. Mean spectra for recording station IW02B (150 m distance to WT 1 of wind farm Tegelberg) for a 2-week period. Only spectra for **(a)** 8 rpm and **(b)** 12.5 rpm are shown. Dashed blue and red lines mark peaks related to multiples of the BPF for 8 rpm and 12.5 rpm, respectively (see Table 2). These frequencies are prominent in the ground motion data, and their amplitude distribution relative to wind direction is shown in Fig. 7.

Each train passage excites a distinct signal, with amplitudes, signal duration, and time-dependent shape related to the specific type of train (local, long-distance, and freight trains) as well as the direction of travel. The distance of the measurement positions relative to the train tracks ranges from 20 to 300 m.

The overall amplitude distribution for each of the five recording stations (at one resident two instruments were installed) is shown in Fig. 8. There is a noticeable difference to the spectra close to the WT (e.g., Fig. 6), as signals related to the eigenmodes of the WTs or the BPF can not be identified. Instead, a clear trend in increased amplitudes can be observed, related to the distance of the measurement position to the train tracks. The closest recording station (IW02G, 20 m distance) reaches PSD values of almost -120 dB (relative to 1 $(\mathrm{m\,s^{-1}})^2\,\mathrm{Hz^{-1}}$) with the maximum at approx. 14 Hz. A decrease in amplitude and peak frequency is found with increasing distance for the frequency range 5–30 Hz. At 300 m distance the maximum is observed at 9 Hz with a PSD value of -140 dB (relative to 1 $(\mathrm{m\,s^{-1}})^2\,\mathrm{Hz^{-1}}$). Differences in the spectra for the indoor and outdoor instruments at resident 3 arise for frequencies above 25 Hz, with lower amplitudes of up to -10 dB indoors. Sharp peaks at approx. 20 Hz, as observed at residents 3 and 4, could be caused by household devices, e.g., a washing machine operating at 1200 rpm.

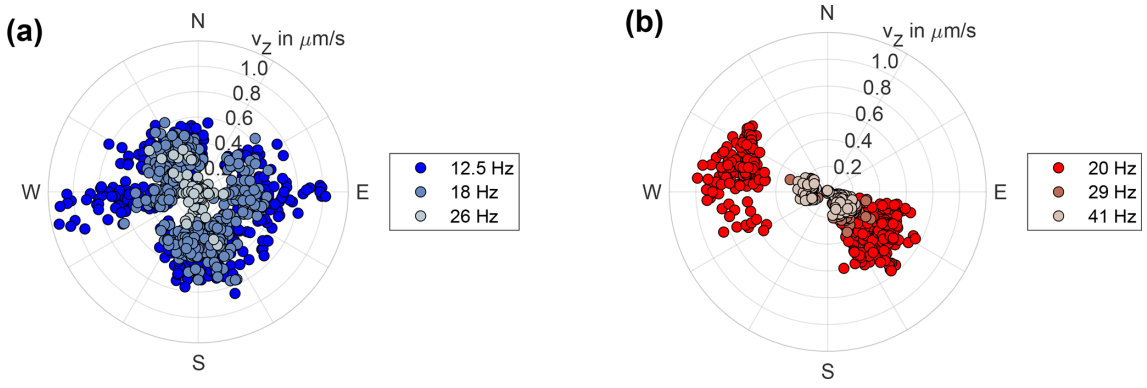

Figure 7. Maximum vertical ground motion amplitudes for 10 min time intervals for the frequencies marked in Fig. 6 for station IW02B (150 m distance to WT 1 of wind farm Tegelberg), depending on wind direction, for **(a)** 8 rpm and **(b)** 12.5 rpm.

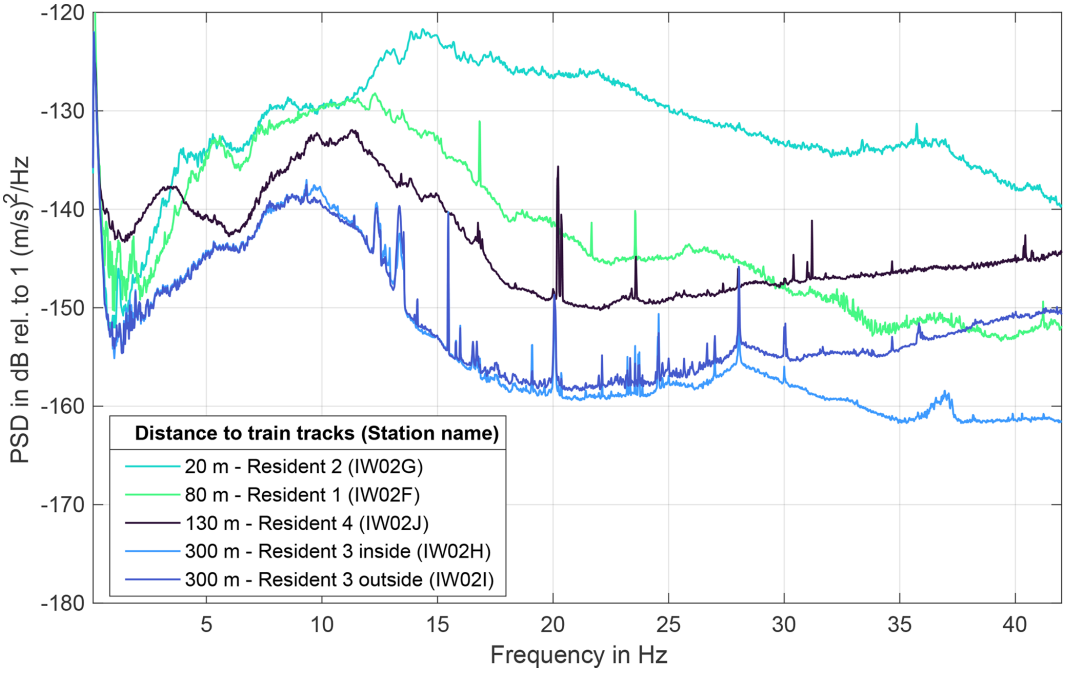

Figure 8. Mean spectra for 8 to 17 d long measurements at residents in the municipality of Kuchen. Amplitude and frequencies exited are closely related to the distance of the measurement location to the train tracks. Two instruments were installed at resident 3, where lower amplitudes are measured in the basement compared to the outside location for frequencies above 25 Hz.

3.3 Comparison to acoustic signals

Side-by-side measurements of ground motion and acoustic signals allow for a direct comparison of how WT emissions and *immissions* manifest in both types of data (as underground and airborne noise). We conducted both types of measurements simultaneously at approximately 150 m distance to WT 1 of wind farm Tegelberg (ground motions – IW02B, acoustics – IMC_A1) and at the four resident sites in Kuchen (ground motions – IW02F-J, acoustic – IMC_B1 (indoor, each resident) and IMC_B2 (outdoor, each resident)). Compared to the ground motion data, where 100 Hz was used as the sampling rate, the acoustic data are sampled with 20 kHz. This allows one to record frequencies of up to 10 kHz, although for the assessment of low-frequency noise only frequencies of 1–200 Hz are considered (Gaßner et al., 2022).

Figure 9 shows time series and spectra up to 45 Hz for 8 h of recording time at the site near WT 1 for 30 October 2020 (compare also Fig. 3 where a shorter section is displayed). We can observe more uniform amplitudes in the ground motion data, while in the pressure data a higher number of transient signals (amplitudes of more than 5 Pa) are visible. Both ground motion and acoustic spectra contain clear signals proportional to the rotation rate at 32 ×, 46 ×, and 64 × BPF. For frequencies below 12 Hz in the ground motion data signals at

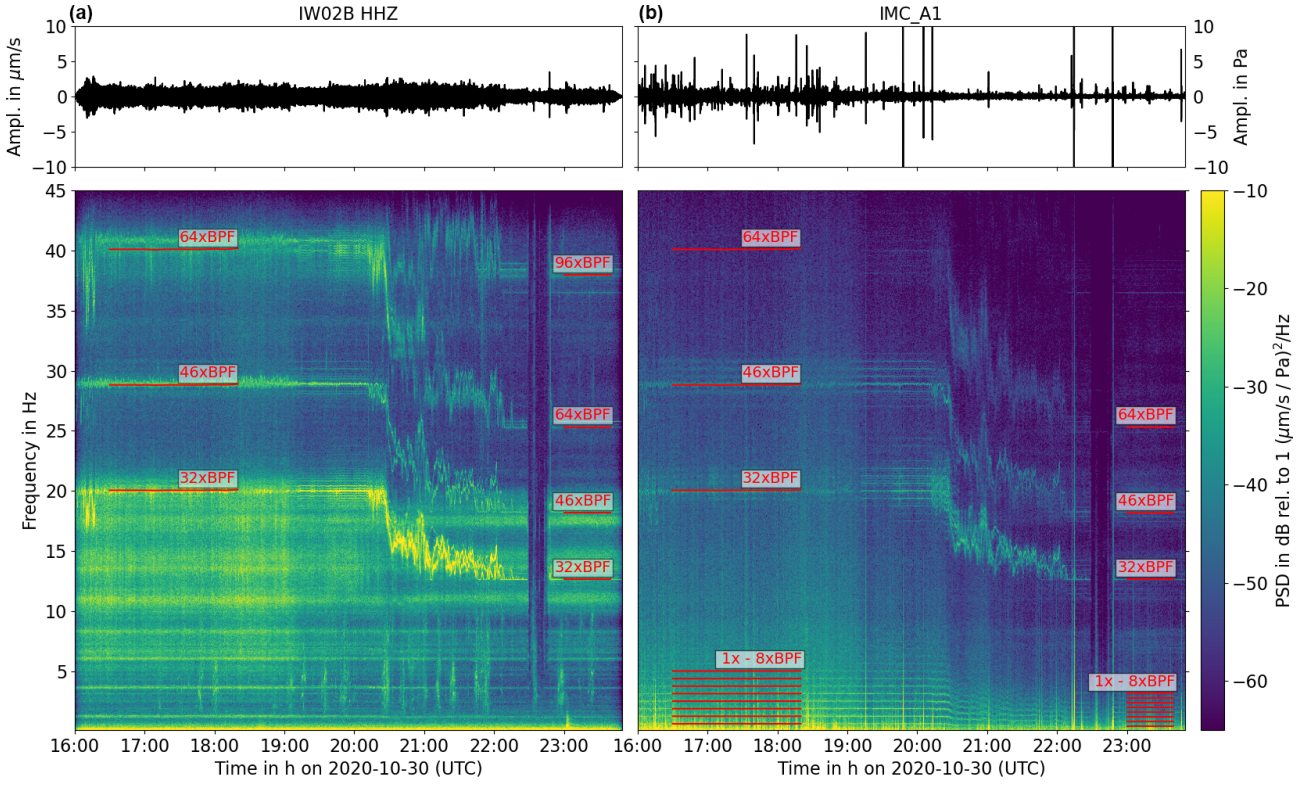

Figure 9. Time series and spectrograms for recording stations IW02B (**a**, vertical ground motion) and IMC_A1 (**b**, sound pressure) at 150 m distance to WT 1 of wind farm Tegelberg for 30 October 2020. A change in rotation rate can be observed at 20:30 UTC and a shutdown of approximately 10 min shortly before 23:00 UTC.

constant frequencies (eigenmodes) can be observed, while in the acoustic data noticeable signals at 1–8 × BPF are visible. Below 10 Hz signals related to the train traffic through Kuchen are also present in the ground motion data but not in the acoustic data.

At resident 1 in Kuchen we can observe WT-related signals for a time window of almost no train traffic on 26 October 2020 from approximately 01:00 UTC to 03:00 UTC (Fig. 10). In the data of all three instruments (ground motion outside the house, acoustic outside and inside) the signal at 32 × BPF can be observed. In the acoustic data also signals at 1–8 × BPF are visible, especially from 04:00 UTC to 08:00 UTC for the outside as well as inside measurements. In the respective ground motion data signals with frequencies at the eigenmodes at 1.2 and 3.6 Hz are present. The train-related signals (starting at approximately 03:00 UTC) are of much higher amplitude compared to the background signals than in the acoustic data and make an identification of WT-related signals almost impossible.

The distribution of maximum amplitudes for signals with frequencies at 32 ×, 46 ×, and 64 × BPF found in the acoustic and ground motion data at the measurement site at 150 m distance to WT 1 is shown in Fig. 11. In the acoustic data the mean of the maximum signal amplitudes decreases uniformly for each rotation rate, while in the ground motion data a different behavior can be observed, with a more significant decrease in maximum amplitudes for frequencies above 20 Hz. This behavior also affects the ratio of the amplitudes, the so-called coupling transfer coefficient C_{AS} (e.g., Novoselov et al., 2020):

$$C_{AS} = \max(A_{seis})/\max(A_{acoustic}). \quad (1)$$

In Novoselov et al. (2020) an acoustic source is studied which produces signals coupled into the Earth. There, the admittance of the signal into the ground can be analyzed directly. Here we study a vibration of the WT that not only causes sound emissions but also transmits signals through the foundation into the subsurface. Possibly, also signals from the air are coupled into the ground, but most likely with a lower proportion. Therefore, it is rather a transmission ratio which we discuss here. Nevertheless, we discuss the respective amplitudes of the signals and stick to the term coupling transfer coefficient. In contrast to Novoselov et al. (2020), we use the maximum amplitudes of 10 min time segments directly, whereas they use envelope amplitudes.

A similar ratio of $C_{AS} \sim 16.5\,\mu m\,s^{-1}\,Pa^{-1}$ can be observed for frequencies of 12.5, 18, and 41 Hz, while $C_{AS} \sim 10\,\mu m\,s^{-1}\,Pa^{-1}$ is found for 20 Hz and $C_{AS} \sim 3$–$5\,\mu m\,s^{-1}\,Pa^{-1}$ for 26 and 29 Hz, respectively. The different amplitude ratios could indicate that additionally acoustic sig-

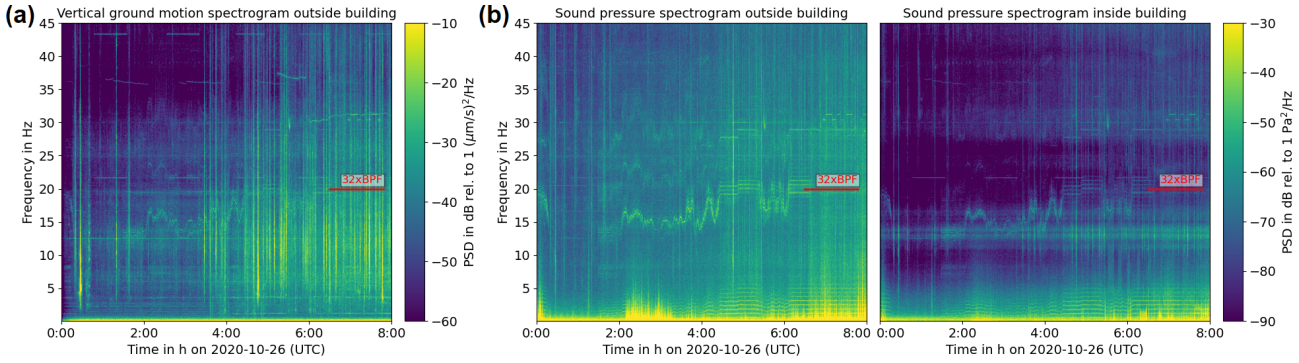

Figure 10. Spectrograms for sites **(a)** IW02F (ground motion) and **(b)** IMC_B1 (acoustic indoors) and IMC_B2 (acoustic outdoors) at resident 1 for 26 October 2020 up to 45 Hz. Signals with frequencies 32 × BPF can be observed in all three data sets. In the ground motion data train signals dominate before 01:00 UTC and after 03:00 UTC.

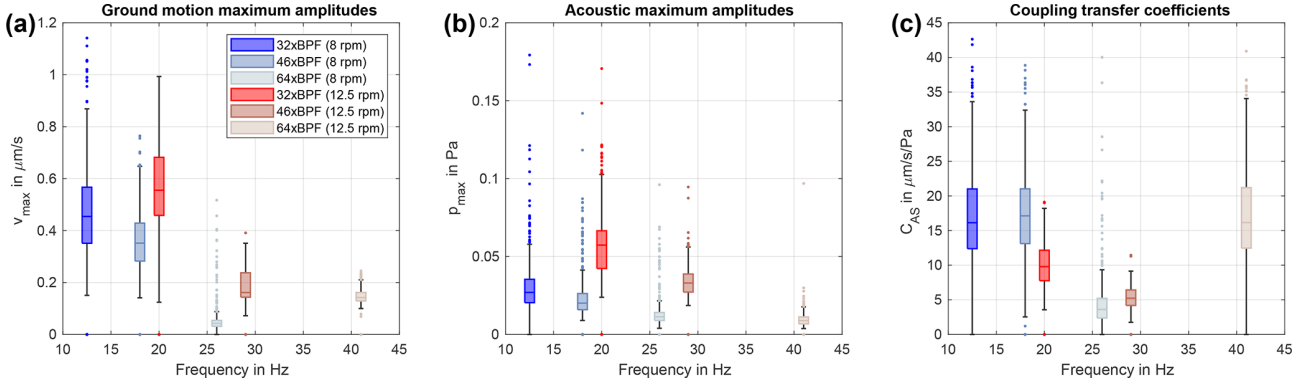

Figure 11. Distribution of maximum **(a)** vertical ground motion and **(b)** acoustic amplitudes for the frequencies marked in Fig. 6 at 150 m distance to WT 1 of wind farm Tegelberg, with **(c)** coupling transfer coefficients C_{AS} according to Novoselov et al. (2020).

nals are coupled into the ground with different admittance for different frequencies (Novoselov et al., 2020) or that properties of the foundation cause lower-amplitude vibrations for frequencies between 20 and 29 Hz.

4 Amplitude decay

An important goal of ground motion measurements in the vicinity of wind farms is the estimation of the amplitude decay rate of the emitted signals (e.g., Stammler and Ceranna, 2016; Zieger and Ritter, 2018; Neuffer et al., 2019; Lerbs et al., 2020; Limberger et al., 2021; Neuffer et al., 2021). Amplitude decay relationships can be used to predict the amplitude of WT-related ground motions in specific distances and, therefore, the influence on sensitive measuring equipment, e.g., seismological sensors. Typically the amplitudes A of the respective PSDs (or rms amplitudes, with $b_{\mathrm{rms}} = 0.5 \cdot b_{\mathrm{PSD}}$), which are measured at instruments along distances r, are fitted by a power-law decay with

$$A \sim 1/r^b. \tag{2}$$

This simple relationship summarizes the different damping relations (geometrical spreading, anelastic and scattering attenuation, and focusing effects) which can hardly be separated. Due to geometric spreading, a value of $b = 0.5$ is expected for the decay of rms amplitudes of surface waves which are most likely the main wave type emitted by WTs Neuffer et al. (2021). In general, b values typically increase for higher frequencies due to frequency-dependent anelastic attenuation and scattering. Therefore, resulting b values are expected to differ significantly for different frequencies and geology, i.e., subsurface complexity and structure.

While varying geology is expected to be responsible for different b values, results from other studies also differ considerably in the approach of fitting amplitude decay curves. The distances considered range between up to 1 km (Neuffer et al., 2021) or at least 1 to 8 km (Stammler and Ceranna, 2016). The chosen distance ranges naturally depend on the study design, available instruments and sites for measurements, and other noise sources (e.g., traffic), but they are a significant factor in the estimation of decay curves. Zieger and Ritter (2018) have shown that b values differ significantly when considering only distances of up to 100 m in-

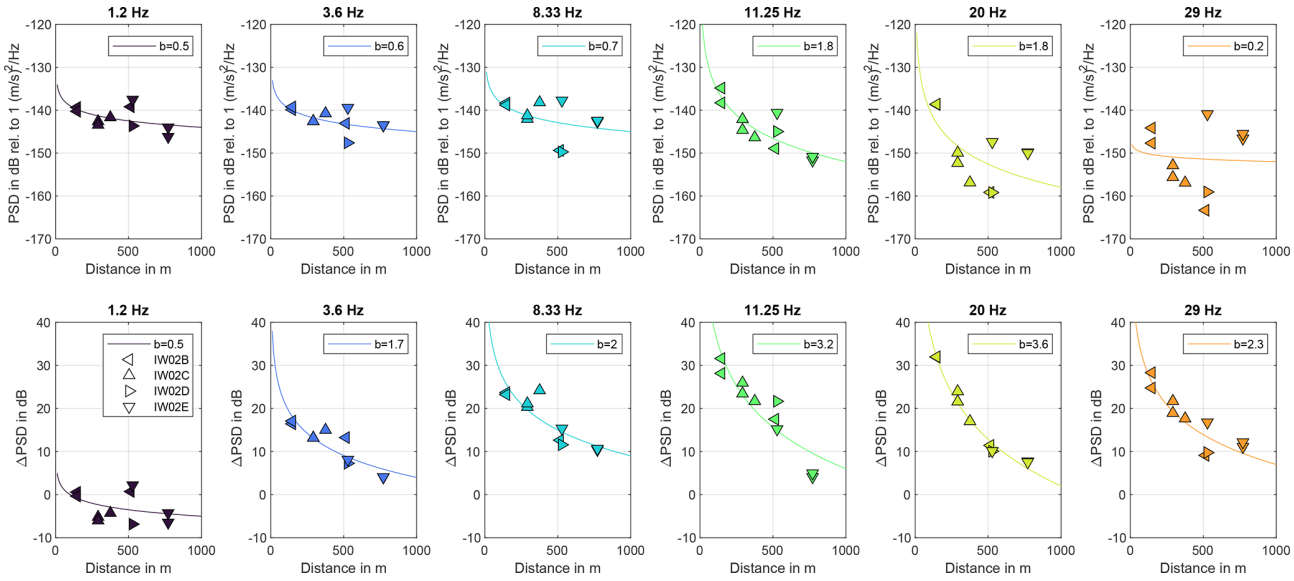

Figure 12. Amplitude decay estimation for three time intervals when only one WT was running at wind farm Tegelberg. Top: amplitude decay for PSD peaks. Bottom: amplitude decay for relative PSD values. The estimated b values are graphically compared in Fig. 15 and are listed in Table 3.

stead of 600 m. Furthermore, measurement times for PSD estimation last from hours (Zieger and Ritter, 2018) to months (Limberger et al., 2021). Stammler and Ceranna (2016) use PSD/N with N the number of considered WTs and take the harmonic mean of WT distances. This approach makes sense in their case, as they take data from stations in large distances of several kilometers to the WTs, where a wind farm can potentially be considered a single signal source. In studies with measurements closer to the WTs mostly the distance to the nearest WT is considered. For example, Zieger and Ritter (2018) and Limberger et al. (2021) use minimum distances (or only one WT) and furthermore the original PSD values without scaling.

Neuffer et al. (2019) use distances to the central WT of the investigated wind farm in their study and take relative PSD values (ΔPSD) to exclude station specific noise effects, which is reasonable if constant noise sources, e.g., traffic, are present. For wind farm Tegelberg, where a railway line is close (Fig. 1), this approach could mitigate the influence related to the distance to train tracks, which is clearly visible in PSD spectra (Fig. 10). For wind farm Lauterstein it might not be necessary to use ΔPSD, as no other prominent constant noise sources can be identified in addition to the WTs. Furthermore, it is more difficult to find a quiet period due to the extent of the wind farm with many WTs and few standstill periods. It also needs to be considered that the background PSD level for evaluation needs to be captured for a representative time; i.e., it should not include strong singular transient events. In this section we compare results for both approaches (PSD and ΔPSD) to estimate amplitude decay relations.

In our evaluation we use six frequencies which comprise eigenmodes (1.2, 3.6, 8.33, 11.25 Hz) and frequencies proportional to the BPF at full load (20, 29 Hz). We use frequency bands of ± 0.4 Hz relative to the center frequencies. Additionally, for wind farm Tegelberg there are three time segments where only a single WT was running. This was either WT 1 (22 and 12 h) or WT 3 (7 h). For these time segments, the direct distance of the recording stations to the respective WT can be used to determine b, leading to distances of up to 800 m. We compare b values calculated directly from the PSD peaks (Fig. 12, top row) to relative PSD values (Fig. 12, bottom row). An improved fit of the PSD values to the amplitude decay curves can be observed for relative PSD values, which we attribute to the influence of the train traffic on seismic amplitudes. The resulting b values can be found in Table 3.

For full operation of both wind farms, we analyze both the maximum PSD values for a 2 d period and those values relative to values for times when the WTs were not running (2 d at wind farm Tegelberg). PSD and ΔPSD are plotted over the minimum distance of the respective instrument to the WTs (Fig. 13). For wind farm Tegelberg these are distances of 150 to 550 m. At wind farm Tegelberg b values of 0.5 at 1.2 Hz to $b = 3.6$ at 20 Hz are found for single WT operation, while for full operation values range between $b = 0.1$ at 1.2 Hz and $b = 4.6$ at 20 Hz (compare Table 3, Fig. 14). Comparing single WT to full wind farm operation, no clear trend can be observed between the respective b values. For 20 and 29 Hz b values for full operation are increased, while b values for 8.33 and 11.25 Hz are reduced. For frequencies of 1.2 and 3.6 Hz b values are similar.

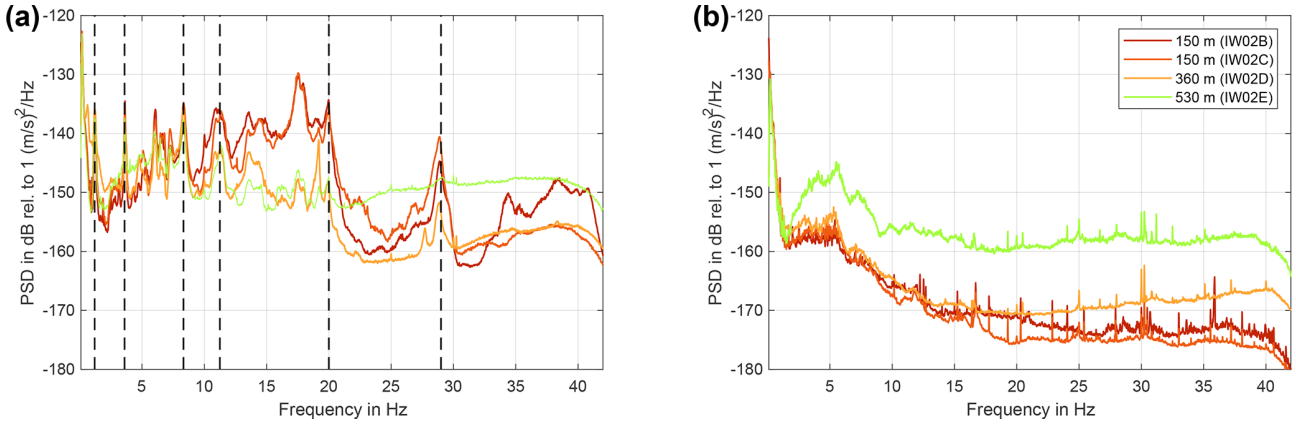

Figure 13. Spectra for amplitude decay estimation for wind farm Tegelberg with three WTs. **(a)** Mean spectra for sites IW02B-E for 2 d of full operation of the wind farm. Frequencies used for amplitude decay estimation are marked by dashed black lines. **(b)** Mean spectra for 2 d without WT operation. Note the increased PSD levels at site IW02E, which is closest to Kuchen and the railway line.

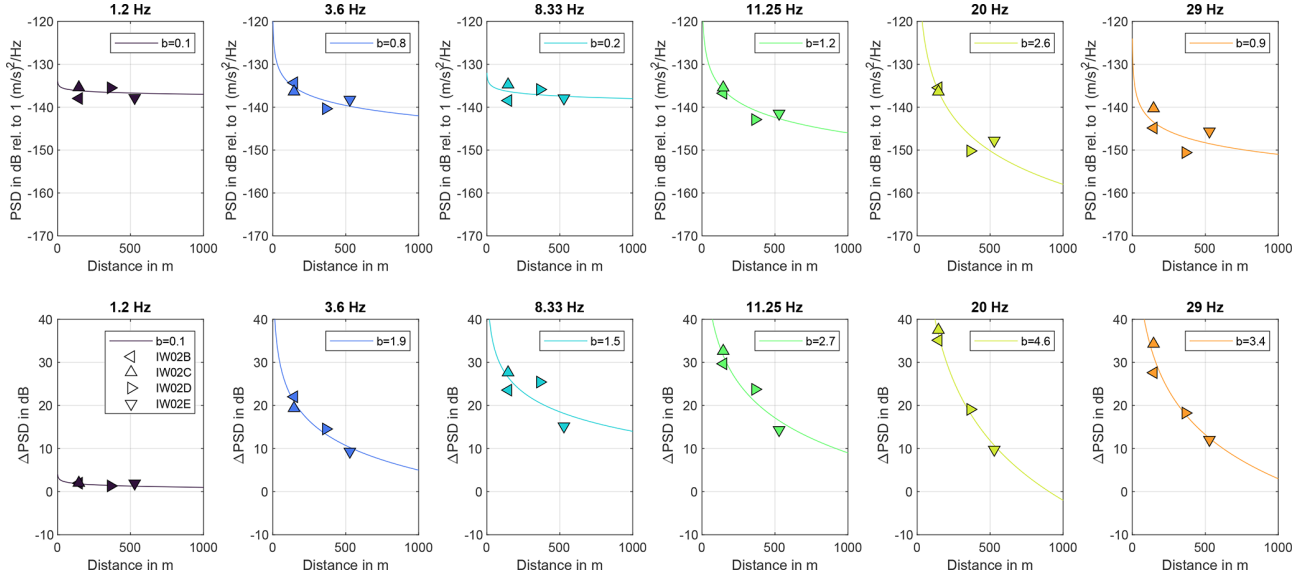

Figure 14. Amplitude decay estimation for full operation at wind farm Tegelberg. Top: amplitude decay for PSD peaks. Bottom: amplitude decay for relative PSD values. The estimated b values are graphically compared in Fig. 15 and are listed in Table 3.

In Fig. 15 b values are compared graphically with symbol sizes proportional to the root-mean-square error (RMSE). The comparison shows that differences in b values are significant for the different approaches, but RMSE values give no clear indication of which approach is to be preferred. We observe no significant difference for 1.2 and 3.6 Hz and a distinct RMSE reduction in b value estimation mainly for 20 and 29 Hz. Figure 16 shows a graphical comparison of the results with literature values. Overall, the results using ΔPSD values give higher b values, fitting better to results from other studies. This confirms the usefulness of the approach for data collected at wind farm Tegelberg where amplitudes are significantly influenced by the train signals.

Results for wind farm Lauterstein are shown in Appendix A in Table A1 and Figs. A1–A3. Only frequencies up to 8.33 Hz are considered here, as higher-frequency signals were not observed in the data at large enough distances (see also Fig. 4). Determined b values are not well restrained, exhibit low b values ($b < 0.5$) or high RMSE (Figs. A2 and A3), and are therefore deemed less significant than the results for wind farm Tegelberg.

5 Discussion

The acceptance of wind energy by society is linked to the understanding of WT emissions which are of acoustic but also of ground motion nature. Such emissions can both be

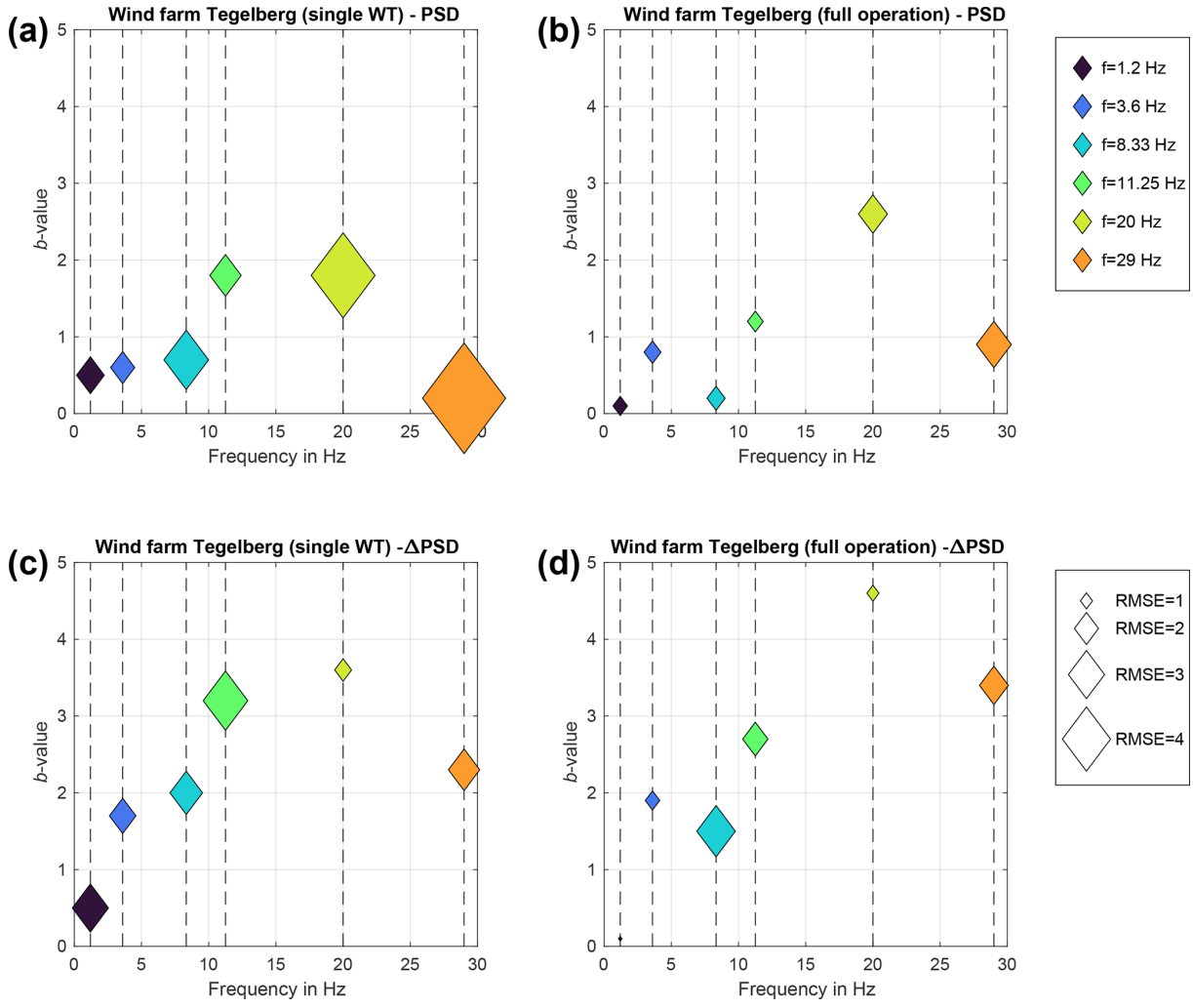

Figure 15. Graphical comparison of b values for **(a)** and **(c)** single WT operation and **(b)** and **(d)** full operation at wind farm Tegelberg. **(a, b)** b values for PSD peaks, **(c, d)** b values for relative PSD. The size of the symbols corresponds to the RMSE of the measured PSD values compared to the theoretical ones from the fitted curves.

Table 3. Amplitude decay b values, comparing the use of PSD and relative PSD values, found for full operation periods for wind farm Tegelberg (1.2 to 29 Hz). Additional results can be determined for single WT operation and are listed for comparison. Literature values are available from other studies in Germany for frequencies from 1.1 to 7.6 Hz, focusing on ground motions due to eigenmode vibrations of the WTs (Fig. 16).

	1.2 Hz	3.6 Hz	8.33 Hz	11.25 Hz	20 Hz	29 Hz
Tegelberg (single WT, PSD)	0.5	0.6	0.7	1.8	1.8	0.2
Tegelberg (single WT, ΔPSD)	0.5	1.7	2.0	3.2	3.6	2.3
Tegelberg (full wind farm, PSD)	0.1	0.8	0.2	1.2	2.6	0.9
Tegelberg (full wind farm, ΔPSD)	0.1	1.9	1.5	2.7	4.6	3.4
	1–3 Hz	3–5 Hz	5–8 Hz			
Fig. 16	0.4–1.1	0.8–2.9	1.6–5.5			

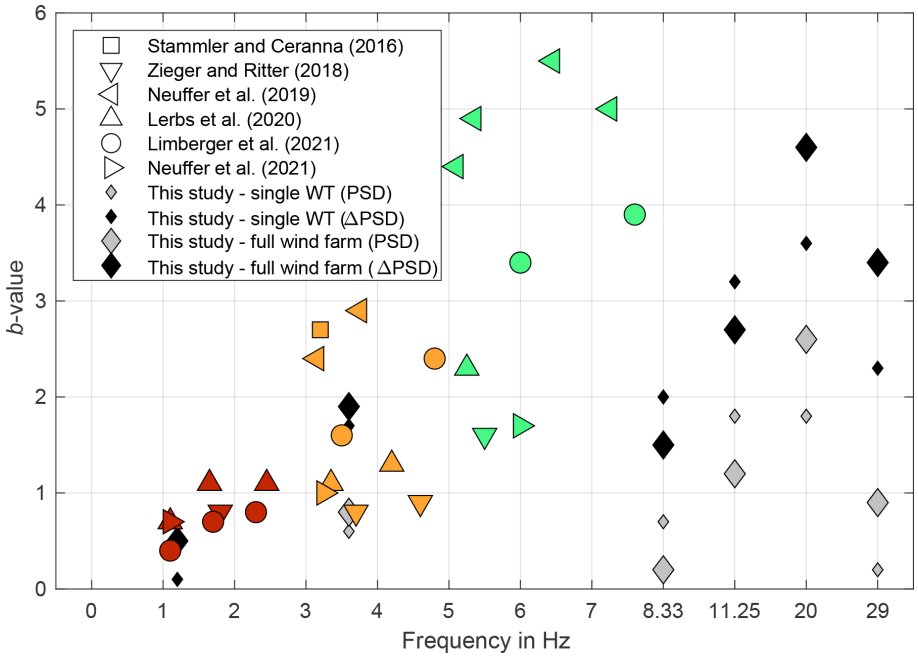

Figure 16. Graphical comparison of published b values from studies discussed in Sect. 4 (red: 1–3 Hz, orange: 3–5 Hz, green: 5–8 Hz). Gray (ΔPSD) and black (PSD) diamond symbols show results for wind farm Tegelberg (Table 3), with smaller symbols indicating the result for a single WT and larger symbols results for full wind farm operation.

recorded in ground motion data due to mechanical coupling with the ground (Figs. 9 and 10). In this study we discuss ground motion emissions of two wind farms consisting of 3 and 16 WTs, respectively (Fig. 1). At sites with 150 to 1900 m distance to the nearest WT, we observe signals below 12 Hz which are related to the eigenmodes of the WT tower and blade rotation. Measurements at different wind farms with the same turbine type confirm that the same frequencies are excited (Fig. 5). The signals increase in amplitude with higher rotation rates (Fig. 6), and we observe 1.2 and 3.6 Hz frequency peaks as far as 2 km distance at wind farm Lauterstein (Fig. A1). Other studies find similar emissions even over distances of several kilometers (e.g., Saccorotti et al., 2011). Measured amplitudes of these eigenmodes (as well as other WT-related signals, Figs. 3 and 4) are at least 1 magnitude lower than the threshold for human perception ($\sim 100\,\mu m\,s^{-1}$). Therefore, local residents are not affected, but ground motions are relevant for sensitive equipment like seismological sensors.

Additionally, signals with frequencies proportional to the BPF above 12 Hz can be observed at distances of up to 1 km (e.g., Fig. 3). These signals are also present in the acoustic data (Fig. 9) and can be related to the WT generator speed and potentially the gears. They are attenuated strongly and, therefore, only affect the direct vicinity of the wind farms but give indications of how WT signals are perceived by residents living near WTs who experience acoustic disturbances. Side-by-side acoustic and ground motion measurements also allow for the identification of other noise sources, especially train traffic in the municipality of Kuchen. We find that it has a much stronger influence on ground motion data than on the acoustic data, though. Furthermore, measured signals reflect short-term changes in WT rotation rate, which potentially capture the attention of residents (especially at night and early morning times, Gaßner et al., 2022) and could be an explanation for reported annoyance, linked to changes in acoustic immissions.

The simultaneous measurement of ground motion and acoustic data allows a detailed analysis and signal amplitude comparison. Amplitude ratios, considering acoustic-to-ground motion coupling as proposed by Novoselov et al. (2020), indicate differing signal strength of acoustic and ground motion signals depending on frequency. In follow-up studies it would be interesting to look at even higher frequencies at co-located measurement sites. Signals with frequencies proportional to the BPF are mainly found in our measurements at wind farm Tegelberg, while at wind farm Lauterstein we observe less dominant signals at higher frequencies due to larger distances (390 to 1900 m) and less superposition of emitted waves because of the wider spatial distribution of WTs.

Amplitude decay relations are important to predict amplitudes at specific distances and are derived from measurements along profiles between the WTs and nearby settlements. We review approaches found in the literature and compare resulting b values for using the maximum PSD values at the studied frequencies or relative PSDs considering a background PSD level when no WTs are running. This is

beneficial especially in the municipality of Kuchen, where a railway line is close and strongly influences ground motion amplitudes at higher frequencies. As stated by Limberger et al. (2021), the latter approach yields increased b values. Our results are in agreement with findings of Zieger and Ritter (2018), Lerbs et al. (2020), Limberger et al. (2021), and Neuffer et al. (2021). To improve the amplitude decay estimation profiles should be measured to the north of wind farm Tegelberg, away from settlements and noise sources like traffic, which would allow a better comparison with other studies.

At wind farm Lauterstein measurements for low-frequency emissions (< 12 Hz) should include larger distances as we expect that the wave field will be highly complex due to the high number of WTs and a superposition of signals in the direct vicinity of the wind farm.

6 Conclusions

We conducted two 108 and 46 d long measurement campaigns to study WT-related signals at two wind farms on the Swabian Alb and at resident sites in nearby communities. Observed signals comprise eigenmodes and signals related to the BPF. In the municipality of Kuchen, in approximately 1 km distance to the wind farm, train traffic is the most significant signal source in the ground motion data. Measured ground motion signals do not have perceptible amplitudes for humans (much smaller than $100\,\mu m\,s^{-1}$) even in the direct vicinity of the WTs.

Furthermore, our measurements were conducted in close proximity to acoustic measurements, allowing for a comparison of WT signals in both types of data. We can identify signals related to the WT generators and gears up to 90 Hz, which are potentially related to annoyance reported by residents and, therefore, provide a helpful data basis to evaluate noise reports. Our comparison of the ground motion and acoustic recordings finds strong similarities above 12 Hz. Thus, recordings with seismometers and high sampling rates may be used in the future to monitor signals in the frequency range of infrasound in the near field of WTs.

At wind farm Tegelberg we observe strong signals with frequencies proportional to the BPF in the vicinity of the wind farm, which are less dominant at wind farm Lauterstein due to the wider station and WT distribution. Higher-frequency signals are attenuated more strongly with distance, which manifests in the amplitude decay. We determine b values for six and three frequencies at wind farms Tegelberg and Lauterstein, respectively. An approach considering relative PSD values is especially beneficial for data from wind farm Tegelberg, where train traffic influences mainly the higher-frequency amplitudes. Nevertheless, significant differences in b values are observed for different approaches, and discussions in the seismological community for a unified data analysis would improve the potential to predict ground motion amplitudes based on different geological settings.

Due to the complexity of wind farm Lauterstein with 16 WTs, the simulation of wave propagation, also considering the 3D topography, could give further indications on how to approach future amplitude decay estimation.

Appendix A: Amplitude decay estimation for Lauterstein

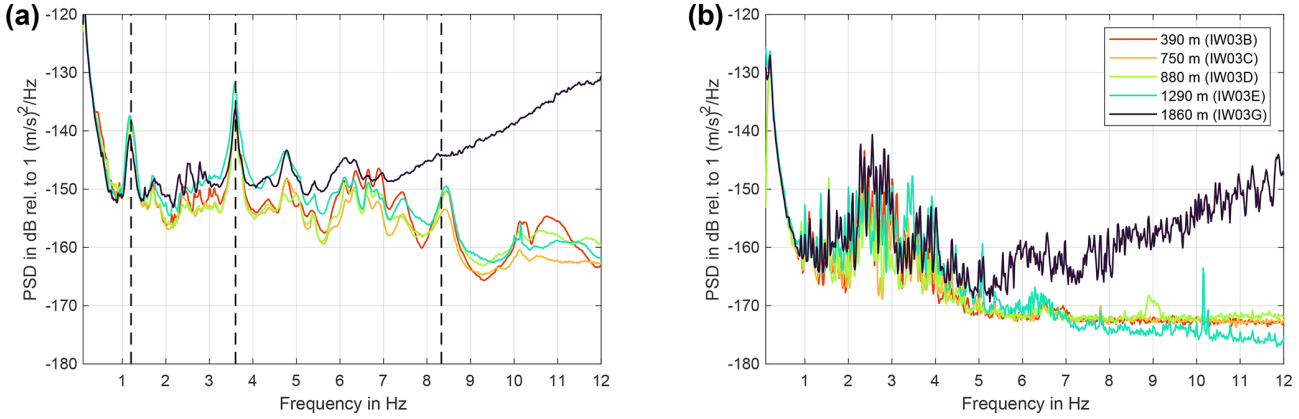

Figure A1. Spectra for amplitude decay estimation for wind farm Lauterstein with 16 WTs. **(a)** Mean spectra for instruments IW03B-E and IW03G for 3 d of full operation of the wind farm. Frequencies used for amplitude decay estimation are marked by dashed black lines. **(b)** Mean spectra for 2.5 h without WT operation. The increased PSD levels at site IW03G for frequencies above 5 Hz originate from a nearby gas heating.

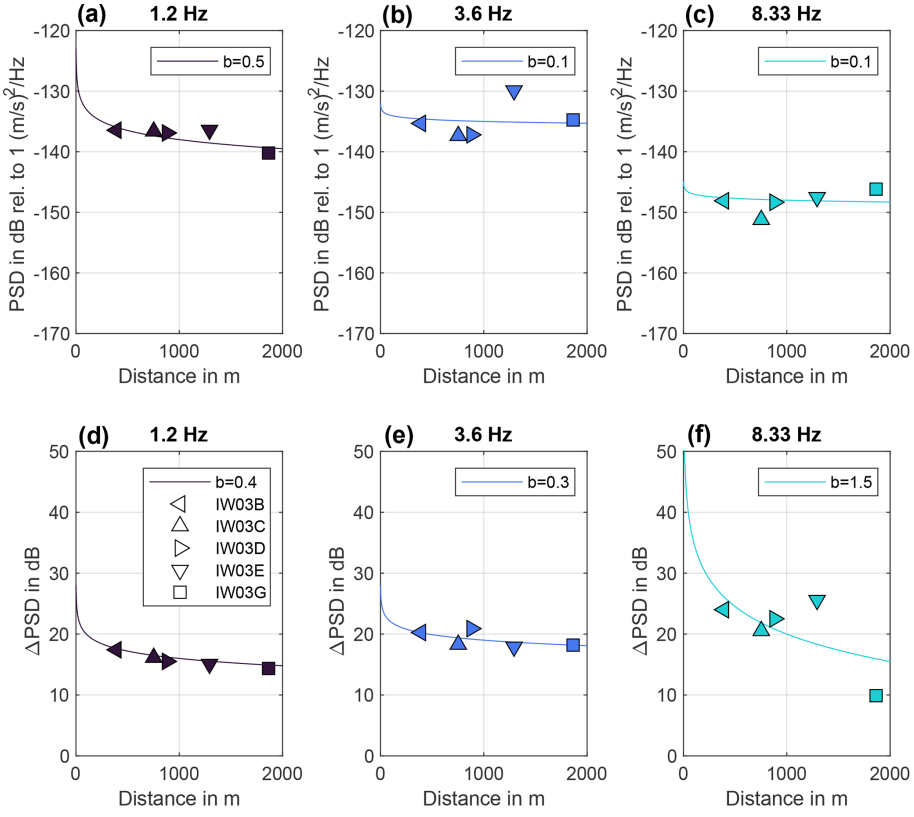

Figure A2. Amplitude decay estimation for full operation at wind farm Lauterstein. **(a)**–**(c)** Amplitude decay for PSD peaks. **(d)**–**(f)** Amplitude decay for relative PSD values. The estimated b values are graphically compared in Fig. A3 and are listed in Table A1.

Table A1. Amplitude decay b values, comparing the use of PSD and relative PSD values, for a full operation period at wind farm Lauterstein (1.2 to 8.33 Hz).

	1.2 Hz	3.6 Hz	8.33 Hz	11.25 Hz	20 Hz	29 Hz
Lauterstein (full wind farm, PSD)	0.5	0.1	0.1	–	–	–
Lauterstein (full wind farm, ΔPSD)	0.4	0.3	1.5	–	–	–

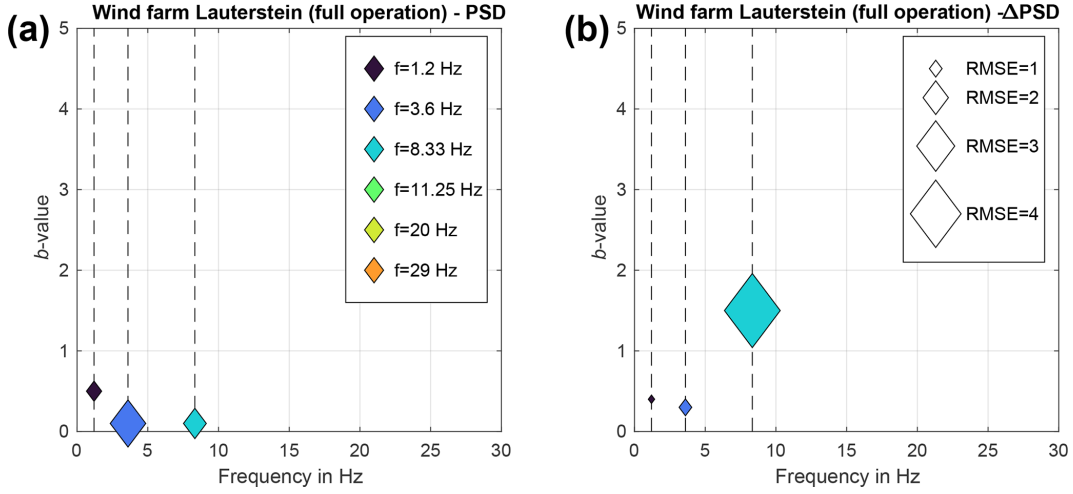

Figure A3. Graphical comparison of b values for full operation at wind farm Lauterstein. **(a)** b values for PSD peaks, **(b)** b values for relative PSD. The size of the symbols corresponds to the RMSE of the measured PSD values compared to the theoretical ones from the fitted curves.

Code and data availability. The code used in this research can be made available upon request; the seismological data will be published after the Inter-Wind project has finished.

Author contributions. LG: conceptualization, data curation, formal analysis, investigation, methodology, software, validation, visualization, writing – original draft. JR: conceptualization, funding acquisition, project administration, resources, supervision, validation, writing – review and editing.

Competing interests. The contact author has declared that none of the authors has any competing interests.

Disclaimer. Publisher's note: Copernicus Publications remains neutral with regard to jurisdictional claims in published maps and institutional affiliations.

Acknowledgements. We thank Susanne Buiter for taking over the editorship and providing helpful suggestions. We are also grateful about the valuable comments from three anonymous reviewers which helped to improve our manuscript. Furthermore, we thank the local authorities of the municipalities of Kuchen and Degenfeld for their support, as well as the Stadtwerke Schwäbisch Hall and KWA Contracting AG for providing access to WT 1 and the WT operating data at wind farm Tegelberg as well as wpd windmanager technik GmbH for access and data related to wind farm Lauterstein. We acknowledge the support of the local residents who allowed the installation of instruments on their property and within their houses. Marie Gärtner and Leon Merkel assisted with the installation of the ground motion sensors. Esther Blumendeller (University of Stuttgart) provided the acoustic data used in this paper. Our study benefits from the excellent cooperation between the Inter-Wind partners from MSH Medical School Hamburg, Martin-Luther-Universität Halle, University of Stuttgart, and the Centre for Solar Energy and Hydrogen Research Baden-Württemberg (ZSW), which is valuable for successful interdisciplinary research.

Financial support. This study is supported by the Federal Ministry for Economic Affairs and Climate Action based on a resolution of the German Bundestag (grant no. 03EE2023D).

Review statement. This paper was edited by Susanne Buiter and reviewed by three anonymous referees.

References

Bundesnetzagentur: Marktstammdatenregister, Bundesnetzagentur, https://www.marktstammdatenregister.de/MaStR/ (last access: 10 Juni 2023), 2022.

DIN 4150-2:1999-06: Erschütterungen im Bauwesen - Teil 2: Einwirkungen auf Menschen in Gebäuden, 2023 Beuth Verlag GmbH, https://www.beuth.de/de/norm/din-4150-2/12168614 (last access: 10 Juni 2023), 1999.

Estrella, H. F., Korn, M., and Alberts, K.: Analysis of the influence of wind turbine noise on seismic recordings at two wind parks in Germany, Journal of Geoscience and Environment Protection, 5, 76–91, 2017.

FA Wind: Hemmnisse beim Ausbau der Windenergie in Deutschland – Ergebnisse einer Branchenumfrage (engl.: Obstacles to the expansion of wind energy in Germany – results of an industry survey), Fachagentur Windenergie an Land, https://www.fachagentur-windenergie.de/fileadmin/files/Veroeffentlichungen/Analysen/FA_Wind_Branchenumfrage_beklagte_WEA_Hemmnisse_DVOR_und_Militaer_07-2019.pdf (last access: 10 Juni 2023), 2019.

Gaßner, L., Blumendeller, E., Müller, F. J. Y., Wigger, M., Rettenmeier, A., Cheng, P. W., Hübner, G., Ritter, J., and Pohl, J.: Joint Analysis of Resident Complaints, Meteorological, Acoustic, and Ground Motion Data to Establish a Robust Annoyance Evaluation of Wind Turbine Emissions, Renew. Energ., 188, 1072–1093, https://doi.org/10.1016/j.renene.2022.02.081, 2022.

Krischer, L., Megies, T., Barsch, R., Beyreuther, M., Lecocq, T., Caudron, C., and Wassermann, J.: ObsPy: A bridge for seismology into the scientific Python ecosystem, Computational Science & Discovery, 8, 014003, https://doi.org/10.1088/1749-4699/8/1/014003, 2015.

Lerbs, N., Zieger, T., Ritter, J., and Korn, M.: Wind turbine induced seismic signals: the large-scale SMARTIE1 experiment and a concept to define protection radii for recording stations, Near Surf. Geophys., 18, 467–482, 2020.

Limberger, F., Lindenfeld, M., Deckert, H., and Rümpker, G.: Seismic radiation from wind turbines: observations and analytical modeling of frequency-dependent amplitude decays, Solid Earth, 12, 1851–1864, https://doi.org/10.5194/se-12-1851-2021, 2021.

Michaud, D. S., Feder, K., Keith, S. E., Voicescu, S. A., Marro, L., Than, J., Guay, M., Denning, A., McGuire, D., Bower, T., Lavigne, E., Murray, B. J., Weiss, S. K., and van den Berg, F.: Exposure to wind turbine noise: Perceptual responses and reported health effects, J. Acoust. Soc. Am., 139, 1443–1454, 2016.

Nagel, S., Zieger, T., Luhmann, B., Knödel, P., Ritter, J., and Ummenhofer, T.: Ground motions induced by wind turbines, Civil Engineering Design, 3, 73–86, 2021.

Neuffer, T. and Kremers, S.: How wind turbines affect the performance of seismic monitoring stations and networks, Geophys. J. Int., 211, 1319–1327, 2017.

Neuffer, T., Kremers, S., and Fritschen, R.: Characterization of seismic signals induced by the operation of wind turbines in North Rhine-Westphalia (NRW), Germany, J. Seismol., 23, 1161–1177, 2019.

Neuffer, T., Kremers, S., Meckbach, P., and Mistler, M.: Characterization of the seismic wave field radiated by a wind turbine, J. Seismol., 25, 825–844, 2021.

Novoselov, A., Fuchs, F., and Bokelmann, G.: Acoustic-to-seismic ground coupling: coupling efficiency and inferring near-surface properties, Geophys. J. Int., 223, 144–160, 2020.

Ratzel, U., Herrmann, L., Westerhausen, C., Bayer, O., Krapf, K.-G., Hoffmann, M., Blaul, J., and Mehnert, C.: Tieffrequente Geräusche inkl. Infraschall von Windkraftanlagen und anderen Quellen, Ministerium für Umwelt, Klima und Energiewirtschaft Baden-Württemberg; LUBW Landesanstalt für Umwelt Baden-Württemberg, Karlsruhe, https://pudi.lubw.de/detailseite/-/publication/84558 (last access: 10 Juni 2023), 2016.

Saccorotti, G., Piccinini, D., Cauchie, L., and Fiori, I.: Seismic noise by wind farms: a case study from the Virgo Gravitational Wave Observatory, Italy, B. Seismol. Soc. Am., 101, 568–578, 2011.

Schofield, R.: Seismic measurements at the stateline wind project, Rept No LIGO T020104-00-/, Laser Interferometer Gravitational Wave Observatory, LIGO, https://dcc-backup.ligo.org/public/0027/T020104/000/T020104-00.pdf (last access: 4 July 2023), 2001.

Stammler, K. and Ceranna, L.: Influence of wind turbines on seismic records of the Gräfenberg array, Seismol. Res. Lett., 87, 1075–1081, 2016.

Styles, P., Stimpson, I., Toon, S., England, R., and Wright, M: Microseismic and infrasound monitoring of low frequency noise and vibrations from windfarms. Recommendations on the siting of windfarms in the vinicity of Eskdalemuir, Scotland, Applied and Environmental geophysics research group, School of Physical and Geographical science, University of Keele, 2005.

Welch, P.: The use of fast Fourier transform for the estimation of power spectra: a method based on time averaging over short, modified periodograms, IEEE T. Acoust. Speech, 15, 70–73, 1967.

Zieger, T. and Ritter, J. R.: Influence of wind turbines on seismic stations in the upper rhine graben, SW Germany, J. Seismol., 22, 105–122, 2018.

Zieger, T., Nagel, S., Lutzmann, P., Kaufmann, I., Ritter, J., Ummenhofer, T., Knödel, P., and Fischer, P.: Simultaneous identification of wind turbine vibrations by using seismic data, elastic modeling and laser Doppler vibrometry, Wind Energy, 23, 1145–1153, 2020.